SHOCK MELTING AND VAPORIZATION OF LUNAR ROCKS AND MINERALS*

THOMAS J. AHRENS
Seismological Laboratory, California Institute of Technology, Pasadena, Calif., U.S.A.

and

JOHN D. O'KEEFE
Dept. of Planetary and Space Sciences, University of Calif., Los Angeles, Calif., U.S.A.

Abstract. The entropy associated with the thermodynamic states produced by hypervelocity meteoroid impacts at various velocities are calculated for a series of lunar rocks and minerals and compared with the entropy values required for melting and vaporization.

Taking into account shock-induced phase changes in the silicates, we calculate that iron meteorites impacting at speeds varying from 4 to 6 km/s will produce shock melting in quartz, plagioclase, olivine, and pyroxene. Although calculated with less certainty, impact speeds required for incipient vaporization vary from ~7 to 11 km/s for the range of minerals going from quartz to periclase for aluminum (silicate-like) projectiles. The impact velocities which are required to induce melting in a soil, are calculated to be in the range of 3 to 4 km/s, provided thermal equilibrium is achieved in the shock state.

1. Introduction

As a result of our intense exploration of the Moon within the last decade, it has become increasingly clear that meteorite impact is an important, if not dominant, process affecting the evolution of the lunar surface. Impact craters are, in fact, the most common, and striking morphological feature appearing on all scales, from microns or so in diameter, to craters easily visible from the Earth, some 1200 km in diameter. The present study of the thermodynamics of shock induced melting and vaporization is motivated by both these considerations, and the observation (Shoemaker *et al.*, 1969; Shoemaker, 1970) that the lunar soil, or regolith, and, probably also, the underlying layers of breccia, are directly, or closely related to the pervasive abundances of shock-induced glasses within these media. Glass in the lunar samples, much of it probably of impact origin, is observed lining micron (Carter and MacGreger, 1970) and millimeter-sized (Hőrz *et al.*, 1971) craters, and as splash-like coatings (Morgan *et al.*, 1971) of what are probably exposed surfaces of lunar rocks. In some cases, these coatings do not have identical compositions to the rocks upon which they are plastered. This suggests that they have an impact origin. The lunar soil is observed to consist of from 10 to 60% glass, depending in general, upon site and core sample (Lunar Sample Preliminary Examination Team (LSPET), 1969, 1970, 1971). The range of composition of these glasses from one-site, is observed to reflect the chemistry of different rocks some of which are in our present compendium of

* Contribution number 210, Division of Geological and Planetary Sciences, California Institute of Technology, Pasadena, Calif. 91109, U.S.A.

Communication presented at the Conference on Lunar Geophysics, held between October 18–21, 1971, at the Lunar Science Institute in Houston, Texas, U.S.A.

analyses (Glass, 1971). The 'whole rock' compositions suggest, the glasses are derived from the whole rock by a rapid process such as impact.

In this paper we examine the impact velocities and meoteroid shock impedances which are required to cause shock melting and vaporization of mineral and rock target materials. Since only the maximum shock conditions produced by a particular impact are considered, the present calculations describe only a relatively small amount of the target material exposed to the maximum shock pressure. Laboratory experiments of Gault *et al.* (1968) demonstrate that nearly all of this material is ejected at later times in the resulting high speed flow. Geometrical arguments, based on the path of rarefaction waves emanating from the lateral and rear surfaces of the impacting meteoroid and the target free-surface, indicate that the mass of material exposed to this maximum shock pressure is on the order of the mass of the meoteroid itself.

In addition to solid materials we also have studied the effect of porosity on lunar materials. This is because the dominant portion, probably over 90%, of the exposed lunar surface is covered with a rubble regolith having bulk densities in the range of 1.3 to 2.3 g/cm^3. LSPET (1969, 1970, 1971). The porosity of the regolith, the numerous breccias which probably underly this rubble in many places, as well as the vesicle porosity of the igneous rocks are expected to have a marked effect on the conditions required for shock melting and vaporization.

The materials of principle interest with regard to the Moon are basalts and their courser-grained equivalents, various pyroxenes, plagioclases, and olivines. Also of interest are silicate materials such as granite which may be the ultimate source of tektites whether this is on the Earth, Moon or on some other solar system body.

2. Shock Thermodynamics

When a meoteroid strikes a surface at speeds which may vary from several kilometers per second, to perhaps 60 km/s, an intense mechanical shock wave is driven forward into the target material and rearward back into the meteorite. In general, this initial shock produces the highest pressure states achieved during the impact process. The intensity of this shock is calculable from knowledge of the Hugoniots (locus of shock states) (Rice *et al.*, 1958) of the target and projectile materials, and the impact velocity. Upon reflection of the rearward propagating shock at the upper surface of the meteorite, a forward travelling rarefaction wave propagates through the meteoroid and subsequently into the target (lunar surface) (Figure 1). This rarefaction wave, and rarefactions emanating from the lateral surface of the projectile and target free-surface, reduce the shock pressure in each mass element of the target. This adiabatic rarefaction process also gives rise to the high particle velocities which cause most of the heavily shocked material to leave the resulting crater as impact ejecta.

In order to determine the range of meteoroid impact velocities sufficient to give rise to melting, or vaporization, of a given rock or mineral, our tactic will be to determine first, the maximum Hugoniot state in the target and then determine whether upon adiabatic expansion, this material remains solid, melts or vaporizes.

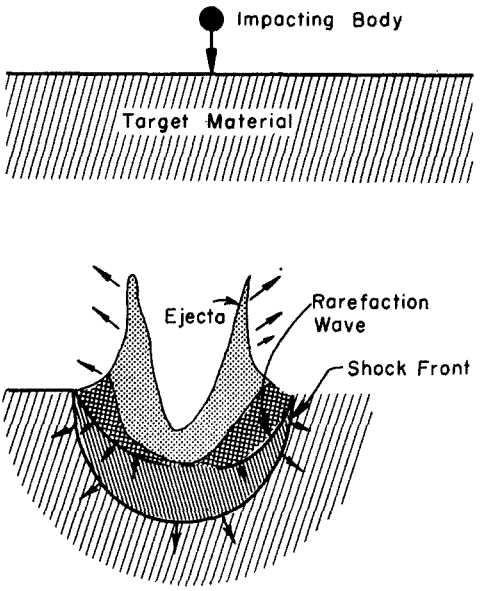

Fig. 1. Generation of shock and rarefaction waves in target material as a result of hypervelocity impact.

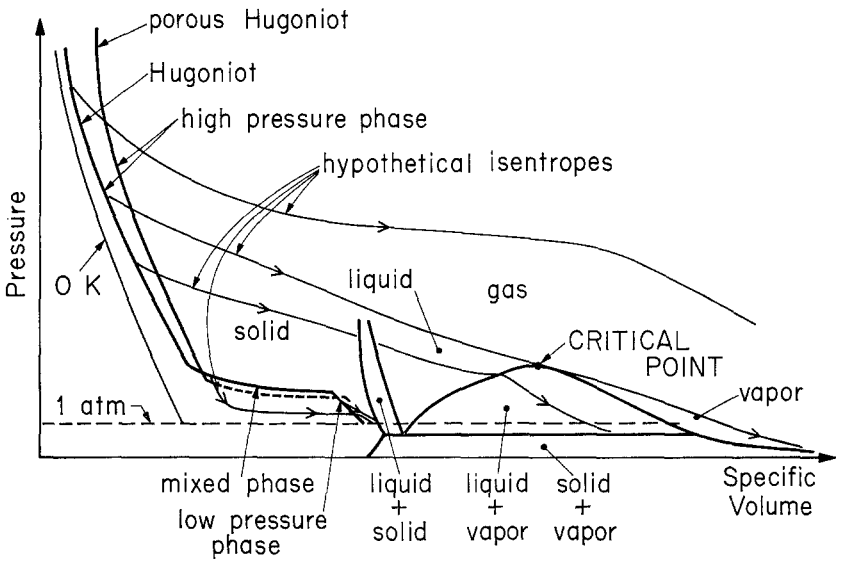

Fig. 2. Pressure-volume relations for a hypothetical silicate which undergoes a shock-induced phase change. The Hugoniot curves which are shown displaying a low-pressure, mixed phase, and high pressure regime are offset by increasing increments of pressure above the O K isotherm by either raising the initial temperature or by increasing the initial porosity. A series of hypothetical release isentropes centered at states in the low and high pressure and mixed phase regimes along the principal Hugoniot are also shown.

The thermodynamic states which result from shock compression to a state on the Hugoniot and subsequent adiabatic expansion for a typical silicate material are shown in Figure 2. All silicates which have been tested to date in the laboratory (including quartz, feldspars, pyroxenes, olivines and garnets (Wackerle, 1962; Trunin *et al.*, 1971a,b; McQueen *et al.*, 1967; Ahrens and Gaffney, 1971; Ahrens and Graham, 1972) display Hugoniot curves similar in shape to that sketched in Figure 2. These Hugoniots reflect the observation that upon shock compression, states corresponding to the initial, or low pressure phase (lpp) are achieved up to pressures on the order of ~ 130 to ~ 300 kb, above which a phase transition(s) in the silicates occur. At successively higher pressures, states in a mixed phase regime in which, with increasing pressure (over a range of 200–400 kb) increasing quantities of a high pressure phase, hpp, (or phases in the case of a rock) coexist with the lpp. At still higher pressures, the Hugoniot curve reflects the pressure (p), volume (V), and energy (e) equation of state of usually a denser polymorph(s) of the mineral, or mineral assemblage. Although the data for many of the silicates are incomplete, it is likely that upon further compression a succession of polymorphs will form, and thus, a number of mixed phase regimes will exist along any one Hugoniot curve. The probable crystallographic nature of the phases which are shock induced in the common silicates are discussed by Ahrens *et al.* (1969a), Davies and Anderson, 1970; Ahrens and Gaffney, 1971; and Ahrens and Graham, 1972.

If the rock or mineral is initially porous, a Hugoniot curve results which, with the possible exception of the mixed phase regime, lies above the solid or principle Hugoniot. Increasing the initial porosity, increases the thermal pressure, at a given volume. Hence the Hugoniots of materials with successively increasing porosity, will be increasingly offset in pressure from the principal Hugoniot. Although extensive measurements of porous Hugoniots have not been carried out for geological materials, with the exception of MgO (McQueen *et al.*, 1971) and SiO_2 (Trunin *et al.*, 1971a,b), such Hugoniots may be theoretically constructed assuming thermal equilibrium and a relation such as the Mie-Gruneisen equation of state

$$p_m - p_h = \gamma (e_m - e_h)/V , \tag{1}$$

where the subscripts m and h refer to the porous, and principal Hugoniot values of the pressure p, and enternal energy, e and γ, the Gruneisen parameter is $V(\partial p/\partial \mathrm{e})_V$. The latter quantity, although in principle experimentally obtainable for all materials, must because of the lack of data, be theoretically estimated for most of the shock induced hpp's.

In order to determine the maximum shock pressure state produced in an initially non porous, or porous, rock or mineral as a result of impact of a stoney (silicate) or iron meteorite, the impedance match method (Rice *et al.*, 1958) is applied. The impedance match method requires knowledge of the Hugoniot curves for both the target and meteoroid, as well as the relative impact velocity. This method, which is strictly applicable only to one-dimensional flows, depends upon the constancy of the normal stress and particle velocity at the target-projectile interface, immediately after

impact in the time period when forward and rearward travelling shocks propagate into the target and projectile, respectively.

Using the impedance-match solution, to determine the high pressure, p-V-e shock state, and using, usually an assumption, regarding the Gruneisen parameter at high pressures, a complete description of the thermodynamic state (including specific entropy, s, and temperature, T) at the condition of maximum compression state is possible (Walsh and Christian, 1955; Ahrens *et al.*, 1969a; Naumann, 1971).

It is more difficult to achieve an adequate description of the final, post-shock states which are achieved by rocks and minerals via adiabatic release along a series of paths (shown diagramatically in Figure 2), largely because of the paucity of pertinent experimental data. For impact velocities of $\sim 5 \times 10^6$ km/s, and lower, radiative transport of energy away from the intensely shocked region on a time scale appropriate to hypervelocity cratering on the moon (10–10^{-9} s) will not be significant (Walsh *et al.*, 1964), and hence the entire shock and rarefaction process within the rock will be closely adiabatic. In general for impact velocities of several kilometers per second and lower, the maximum shock pressure state achieved along the Hugoniots of the silicates, will lie in the lpp regime and the adiabatic release will take place along a path similar to the Hugoniot, but generally lying above the lpp (Walsh and Christian, 1955). Because usually only one phase is involved in this process, the process will be closely isentropic. On the basis of a series of experiments carried out on plagioclase, crystalline and fused quartz (Ahrens and Rosenberg, 1968; Ahrens *et al.*, 1969b; Gibbons and Ahrens, 1971) it appears that adiabatic release from states in the mixed phase regime occurs initially along p-V paths characteristic of the p-V behavior of the hpp. Subsequently, as the pressure is reduced (to values in the ~ 50 to ~ 100 kb range) expansion to a post-shock volume characteristic of the lpp, or, a short-range-ordered material such as maskelynite in the case of plagioclase or amorphous quartz (Milton and DeCarli, 1963; De Carli and Jamieson, 1959) will occur. The result will be a material which has a zero-pressure volume which is greater than that of the lpp crystal material. Release paths from shock states well within the hpp regime have yet to be measured, but the thermodynamic calculations presented below, demonstrate that for release from both the principal and porous Hugoniots, a series of expanded volume, high-temperature states, successively within the solid, solid plus liquid, liquid, liquid plus vapor, and vapor stability fields are to be expected with increasing shock pressure.

3. Calculation of Post Shock Internal Energy

The method most previous workers (Butkovich, 1967; Wackerle, 1962; Ahrens *et al.*, 1969b) have employed in calculating the shock strengths, and hence impact velocities required to induce melting or vaporization upon pressure release, has been to determine, or estimate, the shape of the release adiabats, and then calculate the net gain in internal energy achieved upon shocking and subsequent rarefaction. This energy is h en compared to that required to melt, or vaporize, the material at low pressure.

The post-shock energy is given

$$e_p = e_0 + \tfrac{1}{2}p_h(V_0 - V_h) - \int_{V_h}^{V_{00}} (p\,\mathrm{d}V)_s, \tag{2}$$

where e_0 and V_0 are the initial pre-shock internal energy and specific volume, V_h and V_{00} are the Hugoniot and post-shock volume. In Equation (2) the shock state is assumed to be achieved via a single shock discontinuity. The integral is taken along the release adiabat which is assumed to be an isentrope. In our view, the major advantage of this procedure is that it requires no additional information regarding the Gruneisen parameters if measured release adiabats are available. However, if these release data are not measured, as in the case of complex behaving silicates, they are difficult to calculate theoretically with any degree of confidence.

As an example, we have applied Equation (2) to the Hugoniot and release data of Ahrens *et al.* (1969b) for the Muskwa Lake oligoclase. This mineral has a composition equivalent to 75.1% albite, 19.4% anorthite and 5.5% orthoclase. As shown in Figure 3, release adiabats centered at Hugoniot states at 180, 272 and 416 kb were measured. The states at the two, lower pressures, are thought to lie in a mixed phase regime, representing a mixture of oligoclase and either a mixture of jadeite, grossularite,

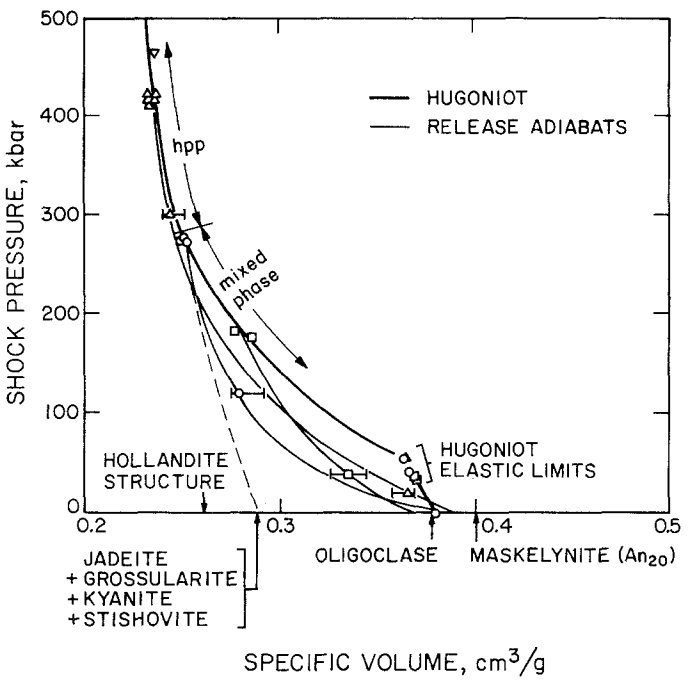

Fig. 3. Experimental Hugoniot and release adiabats for Muskwa Lake oligoclase. Horizontal error bars represent experimental uncertainties (after Ahrens *et al.*, 1969b).

kyanite and SiO_2 (coesite or stishovite) or perhaps a hpp of oligoclase in the hollandite structure (Ahrens *et al.*, 1969a). The Hugoniot state at 416 kb, probably corresponds to nearly complete transformation to the hpp(s). By applying Equation (2) to the measured release adiabats, and their rather large experimental uncertainties, the post-shock energy gains, plotted in Figure 4 are obtained. Ignoring the small difference between internal energy and enthalpy at ambient pressure, a temperature scale, corresponding to the enthalpy versus temperature data (Robie and Waldbaum, 1968) for plagioclases is also shown in Figure 4. As can be seen from the figure, within the

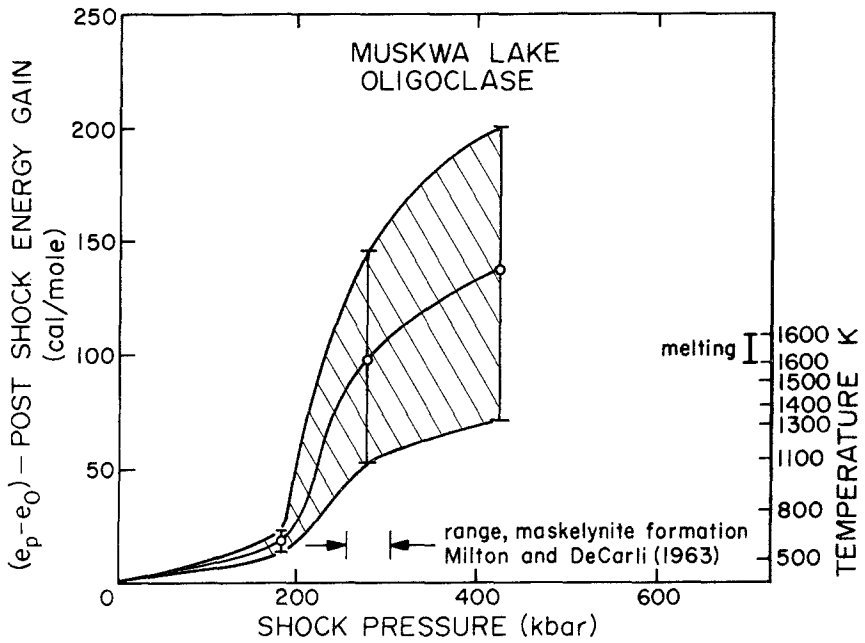

Fig. 4. Calculated post-shock energy gains, versus shock pressure from the experimental release adiabat data of Figure 3.

experimental uncertainties, the melting interval we infer for this composition, overlaps the range of maskelynite formation (shock-induced amorphous phase) reported by Milton and DeCarli (1963). However, in the reflected shock geometry of Milton and DeCarli, their peak temperatures were much lower and subsequent experimentation has indicated that maskelynite may form as low as 150 kbar which corresponds to energies well below those required for melting. The post-shock temperatures calculated here are considerably greater than originally estimated by Ahrens *et al.* (1969b).

4. The Post-Shock State Using the Entropy Method

The method of calculating entropy along the Hugoniot (Zeldovich and Raizer, 1966; Ahrens, 1972), and comparing the resulting values with the entropies required to melt

or vaporize a material at low pressure and high temperatures has apparently been overlooked by previous workers concerned with geological materials. In applying this simple idea, it is of course, implicitly assumed that all the entropy production takes place during the shock process, and during the rarefaction process the specific entropy remains constant. The tactic which is followed is to determine the entropy increase resulting from shock compression of both initially nonporous, and a series of distended minerals, and rocks, and compare the entropy values, to the entropy versus temperature, measured or calculated, for the solid, liquid and vapor phase at one atmosphere. In general, the differences in entropy of the solid polymorphs are usually much smaller than the entropy changes associated with vaporization. In the case of vaporization on the Moon we are interested in the entropies at $<10^{-10}$ T, however the isentropes which lead to vaporization will of course also pass through a one atmosphere state. In cases where the isentrope passed through the vapor dome (Figure 2) we will underestimate the amount of either solid or liquid coexisting with the vapor. However for shock states having entropies much greater than that existing at the liquid-vapor critical point, where most of the material will remain gaseous, even at very low pressures our estimates of the shock states required for vaporization based on calculations at ambient pressure, should be fairly valid. Entropies required for melting of different minerals are taken from thermodynamic tabulations (Table I). The entropies required for incipient and complete vaporization which are also shown in the table are calculated theoretically by the methods described in the next section.

Except for periclase, all of the rocks and minerals studied undergo a shock-induced phase change in the regimes experimentally studied. Because sufficient entropy to melt the lpp's of these are only achieved either, within, or above the range of hpp Hugoniot data, we have considered only the latter regime in our analysis. Employing the calculated temperature along the principal hpp Hugoniot reported by the various authors indicated in Table I, the entropy at any point along the hpp principal Hugoniot is given by

$$\Delta s_h = \int_0^{T_h} C_v(\theta_D/T)\frac{dT}{T}. \tag{3}$$

By calculating the variation in θ_D, the Debye temperature, at each Hugoniot volume V_h, and using the Gruneisen parameter for the high pressure phase, the specific heat at constant volume, C_v, the entropy along the Hugoniot is obtained using the calculations given by Furakawa and Douglas (1963). Since the shock temperatures in the hpp regimes are comparable, or generally exceed, the Debye temperatures above ~ 500 kb (for the nonporous materials) the major uncertainties in the above procedure stem largely from the uncertainties in the calculated Hugoniot temperatures rather than failure of Debye theory (Kieffer and Kamb, 1972) in describing the thermal properties of silicates. The uncertainties in T_h, which are on the order of $\sim 25\%$ at compressions of 0.8, and probably approach $\sim 50\%$ at compressions of 0.6, reflect the uncertainty in the Gruneisen parameter.

TABLE I

Summary of hugoniot data used for calculating shock melting and vaporization

	Zero-pressure density		Range of experimental data				Mean atomic weight $\bar{M}$	Gruneisen ratio γ_0	Debye temperature K
	ρ_0(1pp) (g/cm^3)	ρ_0(hpp) (g/cm^3)	P_{min} (Mbar)	P_{max} (Mbar)	$(V/V_0)_{max}$	$(V/V_0)_{min}$			
Bamle Enstatite[a]	3.277	3.67	0.402	1.061	0.77	0.69	21.2	1.0	928
Twin Sisters Dunite[b]	3.32	4.12	0.607	1.105	0.68	0.64	20.9	0.82	676
Hortonolite Dunite[b]	3.79	4.75	0.816	1.209	0.68	0.62	25.1	0.69	1309
Stishovite[b]	2.654	4.284	0.256	1.995	0.58	0.48	20.03	0.995	1141
Oligoclase[c]	2.634	3.69	0.336	0.705	0.62	0.58	20.49	1.0	935
Periclase[b]	3.584	3.584	0.199	1.225	0.91	0.71	20.16	1.6	887
Anorthosite[d]	2.73	3.53	0.200	1.200	0.63	0.55	21.0	1.13	881
Vacaville Basalt[e]	2.65	4.04	0.201	1.836	0.64	0.51	22.9	1.39	1055
Frederick Diabase[d]	3.01	3.37	0.200	1.200	0.73	0.58	21.50	1.19	829
Westerly Granite[d]	2.63	3.82	0.200	1.200	0.60	0.53	20.60	1.05	797
Centerville Diabase[d]	2.98	3.47	0.200	1.200	0.70	0.57	21.80	1.10	867

[a] Data from Ahrens and Gaffney (1971).
[b] Data from McQueen *et al.* (1967), analysis, Ahrens *et al.* (1969a).
[c] Ahrens *et al.* (1969b).
[d] Data and analysis from McQueen *et al.* (1967).
[e] Data from Jones *et al.* (1968).

The pressure along the porous Hugoniot is calculated from Equation (1) and the conservation of energy Rankine-Hugoniot relation (Rice *et al.*, 1958) and is given by

$$p_m = p_h \left[\frac{1 - \frac{\gamma}{2}\left(\frac{V_0}{V} - 1\right)}{1 - \frac{\gamma}{2}\left(m\frac{V_0}{V} - 1\right)} \right]. \tag{4}$$

The temperature along the porous Hugoniot is given by

$$T_m = T_h + \frac{(p_m - p_h)\, V}{3R\gamma}. \tag{5}$$

In Equation (5) the Dulong-Petit value of C_v is assumed. Here m is the distention of the initial (lpp) material of crystal volume V_0. Hence the initial volume of an initially porous mineral or rock is given by mV_0. Equations (4) and (5) are valid as long as the Gruneisen ratio depends only on volume, and the compressions are less than that at which $\partial p_h/\partial V = -\infty$ or the condition

$$\frac{V}{V_0} = \frac{\gamma m}{2 + \gamma} \tag{6}$$

occurs.

In Equations (4)–(6) it is assumed that the porous medium has come to thermal equilibrium in the shock state. For a grain size on the order of 0.1 mm, characteristic thermal conduction times are $\sim 100\ \mu$sec for silicates. However if local radiative energy transfer between grains occurs, the thermal equilibrium time will be drastically reduced.

5. Entropy of Vaporization of Silicates

In simple materials such as metals, the minimum value of the entropy, in which all bonds are just broken is the value of the entropy at the critical point (Figure 2). In the more complex silicates, this is not a very convenient criteria since the vaporization process is incongruent, and the critical point, if it exists, is difficult to determine. A critical point calculation is only attempted in the case of SiO_2 (next section) for which some data on the pertinent species at high temperature are available from the work of Porter *et al.*, 1955. As discussed in the previous section, upon adiabatic expansion into a vacuum, a mass element of the shocked material will always pass through the state corresponding to 1 A pressure* and the entropy at this state provides a measure of whether vaporization can be achieved at this mass element. This measure will not in general give the absolute minimum value of entropy for vaporization, since there can always be shock states in which vaporization occurred upon expansion, and subse-

* This may not, however, be an equilibrium state.

quently condensation, ensued at a pressure greater than one atmosphere. However, the range of states for which this may occur is fairly narrow. The key unknowns in calculating the entropy at 1 A pressure are the final temperature at which the last constituent vaporizes and the molecular species of the vapor.

Kreiger (1967) has performed detailed high temperature thermodynamic calculations on several complex materials and two minerals, quartz and enstatite. He found that enstatite disproportionated into the oxides MgO and SiO_2. These oxides have temperatures of vaporization at 1 A of approximately 3350 K and 3175 K respectively. Kreiger found that the temperature at which the individual oxide component leaves (boils off) the mineral, upon heating, does not vary significantly from the vaporization temperature of the pure oxide (Figure 5). As suggested by Kreiger's result, we will

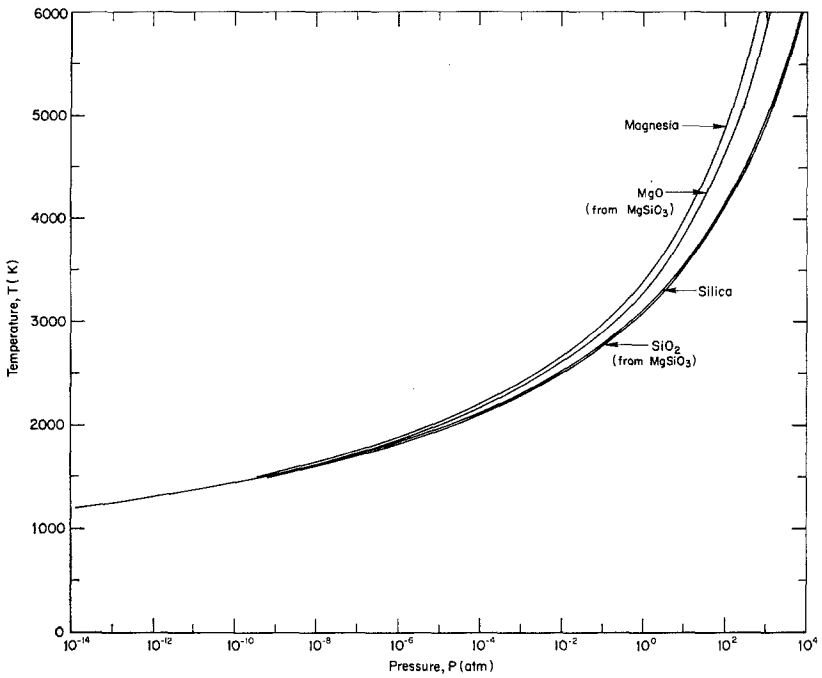

Fig. 5. Calculated sublimation temperature of magnesia (MgO) and silica (SiO_2) separately, and in the presence of each other, in the mineral enstatite ($MgSiO_3$), after Krieger (1967).

assume for all the silicates that the temperature at which the liquid is completely converted to vapor, is the highest temperature of vaporization represented by the constituent oxides. This assumption therefore ignores any nonideal solution effects. A list of the temperatures of vaporization of important oxides (Table III) was obtained from the review paper by Brewer (1953). With the knowledge of the vaporization temperature and gaseous species, the entropy can be calculated using the methods of statistical mechanics (Mayer and Mayer, 1940). For each of the atomic and diatomic

TABLE II

Entropy values for minerals

	Melting point (°K)	Incipient melting entropy (cal/mole-atom K)	Complete melting entropy (cal/mole-atom K	Approximate vaporization temperature (K)	Incipient vaporization entropy (cal/mole-atom K)	Complete vaporization entropy (cal/mole-atom K)
SiO_2	1996[a, b]	13.40[a, b]	13.73[a, b]	3175[f]	17.0[e]	34.9
MgO	3125[a]	17.12[c, a]	–	3350	16.3[f]	35.9 36.0[e]
Mg_2SiO_4	2163[a]	14.24[a]	–	3350	17.6	35.6
Fe_2SiO_4	1490[a]	14.43[a]	16.54[a]	3400	21.8	36.2
$MgSiO_3$	1830	12.85[a]	14.46[a] 14.85[e]	3350	18.9 18.6[e]	35.5
$FeSiO_3$	–	–	–	3400	19.6	35.9
$CaMgSi_2O_6$	1664[a]	12.70[a]	13.81[a]	3800	21.3	36.2
$CaFeSi_2O_6$	–	–	–	3800	22.6	36.4
$KAlSi_3O_8$	1473[c, a]	12.69[c, a]	13.46[c]	3800	21.1	37.0
$NaAlSi_3O_8$	1391[d, a]	12.18[d, a]	12.93[d]	3800	21.5	36.9
$CaAl_2Si_2O_8$	1825[c, a]	13.61[a]	–	3800	17.7	36.1

[a] From Robie and Waldbaum (1968).
[b] For cristobolite.
[c] For high sanidine.
[d] For high albite.
[e] From JANAF tables.
[f] Unlabeled values are calculated or inferred.

species, the individual contribution the total entropy is given by

$$S_i = S_{el} + \tfrac{7}{2}R + R \ln \left(\frac{2\pi m k T}{h^2} \right)^{3/2} \frac{V}{N} + R \ln \left(\frac{8\pi^2 \mu r^2 k T}{h^2} \right) + \frac{Rhv}{kT} \frac{1}{\exp\left(\frac{hv}{kT} \right) - 1} - R \ln \left\{ 1 - \exp\left(- \frac{hv}{kT} \right) \right\}, \tag{7}$$

where S_{el} is the electronic contribution (Lewis and Randall, 1961) and R, k, h and N is the gas, Boltzmann, Planck and Avagadro's constants, and m, μ, r and v are the molecular mass, reduced mass, interatomic spacing and vibrational frequency. The values of the latter molecular constants were taken from Dieke (1963). The resulting entropies for complete vaporization are given in Table II.

TABLE III

Assumed vaporization products for silicates

Silicate	Oxide gas
SiO_2	$\rightarrow SiO + 1/2\ O_2$ [a]
$MgSiO_3$	$\rightarrow MgO + SiO + 1/2\ O_2$
Mg_2SiO_4	$\rightarrow 2MgO + SiO + 1/2\ O_2$
$CaAl_2Si_2O_8$	$\rightarrow CaO + 2AlO + 2SiO + 3/2\ O_2$
$NaAlSi_3O_8$	$\rightarrow Na + AlO + 3SiO + 2\ O_2$
Fe_2SiO_4	$\rightarrow 2FeO + SiO + 1/2\ O_2$
$CaMgSi_2O_6$	$\rightarrow CaO + MgO + 2SiO + O_2$
$CaFeSi_2O_6$	$\rightarrow CaO + FeO + 2SiO + O_2$
$NaAl(SiO_3)_2$	$\rightarrow Na + AlO + 2SiO + 3/2\ O_2$
$KAlSi_3O_8$	$\rightarrow K + AlO + 3SiO + 2\ O_2$

[a] Porter *et al.* (1955).

The increment in entropy from incipient to complete vaporization was calculated from

$$\Delta S = \frac{H_v}{T_v}, \tag{8}$$

where H_v is the enthalpy of vaporization and T_v is the temperature of vaporization. For the minerals being considered, incongruent vaporization occurs over a range of temperatures. A lower bound on the entropy increment was determined by taking T_v to be the temperature at which the vaporization process is completed, i.e. the vaporization temperature of the most refractory oxide. The following thermodynamic cycle for enstatite was typical of those used for calculating the enthalpy of vaporization (Figure 6).

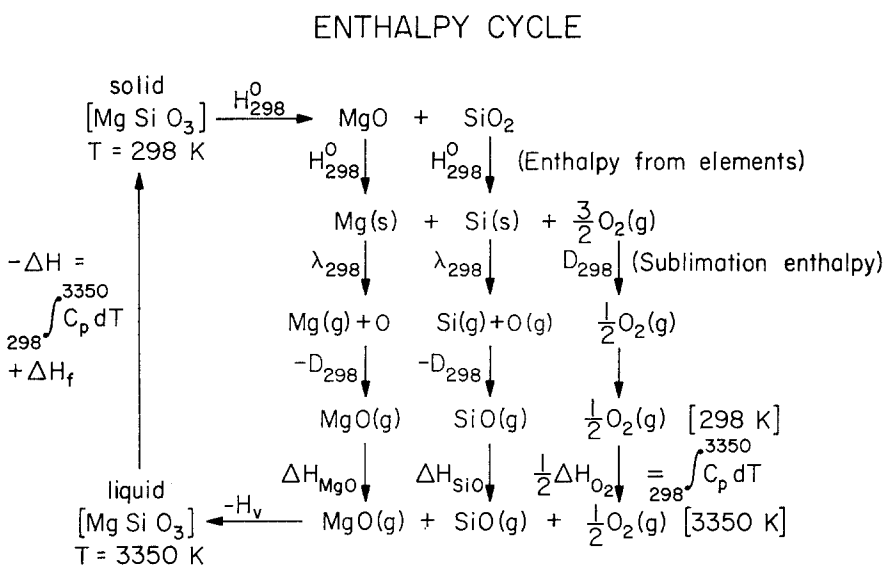

Fig. 6. Typical enthalpy cycle used to calculate heat of vaporization. The example is $MgSiO_3$ where H_{298}, λ_{298}, and D_{298} are the heats of formation, sublimation and dissociation at 298.15 K, respectively and H_v is the unknown heat of vaporization.

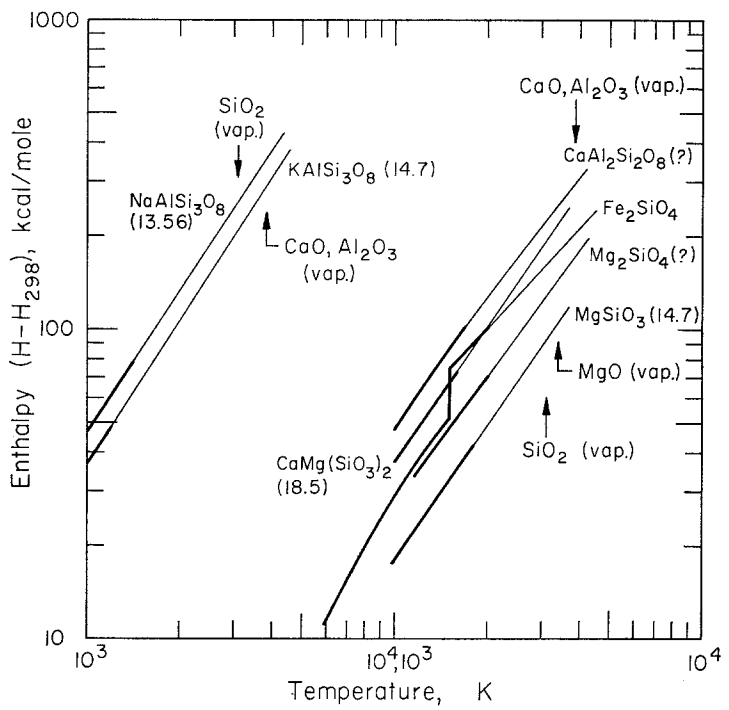

Fig. 7. Enthalpy versus temperature, at ambient pressure for silicates used in shock melting calculations. Heavy lines indicate data compiled in Robie and Waldbaum (1968). Light lines are extrapolated. Numbers in parentheses are heat of fusions, (vap.) indicates incipient vaporization.

Starting with the solid at 298 K and proceeding in a clockwise manner, the first enthalpy change entails the heat of formation of the crystal from the oxides, then the heat of formation of the oxides from the elements in their standard states, the sublimation of the solids to gases, and the reaction of the gases to form the vapor species expected from the vaporization process. All of the above processes were considered at 298 K. The heats in each of these, were obtained from compilation of thermodynamic properties in Robie and Waldbaum (1968). The next enthalpy change in the cycle is the heat required to raise the various species to the temperature of vaporization. This enthalpy was calculated using the statistical mechanical formulae for the temperature dependence of the specific heat at constant pressure (Mayer and Mayer, 1940) and spectroscopic data for the molecular parameters (Dieke, 1963). The enthalpy required to convert the liquid at 3350 K (temperature of vaporization of MgO) to the vapor at that temperature was defined as the unknown heat of vaporization. The remaining step in the cycle was the energy required to heat crystal from 298 K to the melting point, completely melt and heat the liquid to the vaporization temperature. The thermodynamic compilations of Robie and Waldbaum were used in these calculations for temperatures up to 2000 K and for temperatures above 2000 K these data were graphically extrapolated and in some cases the heats of fusion were estimated (Figure 7). The resultant values for the change in entropy upon complete vaporization were then calculated from Equation (8) and used to determine the entropy for incipient vaporization shown in Table II.

6. The Critical Point for SiO_2

The position of the vapor-liquid critical point of SiO_2 can be calculated using the recent theory of Young and Alder (1971), in which the gaseous phase is assumed to obey a modified van der Waal's equation of state. In this theory, the van der Waal's constant, a, is determined in the usual way from the liquid specific volume, V_L, and cohesive energy of the liquid, E_0, relative to the gas species, $a = -E_0 V_L$. The van der Waal's constant b is determined from the Percus-Yevick expression relating the hard sphere diameter σ, to the volume of the liquid at the melting point,

$$\sigma^3 = 0.45 \frac{6V_L}{\pi N}. \tag{9}$$

In these terms b is given by

$$b = \tfrac{2}{3}\pi N \sigma^3. \tag{10}$$

The expressions for the critical constants are

$$\begin{aligned} V_c &= 2.417 \times 10^{24}\, \sigma^3, && \text{(a)} \\ P_c &= 0.2596\, a/V_c^2, && \text{(b)} \\ T_c &= 0.7232\, a/RV_c. && \text{(c)} \end{aligned} \tag{11}$$

TABLE IV

Calculated critical point properties of SiO_2 theory of Young and Alder (1971)

Parameter	Value
V_c	1.57 cm^3/g
P_c	6.42 kb
T_c	13,500 K
a	9.75×10^{13} ergs $cm^2/mole^2$
b	0.818 cm^3/g
S_c	22.6 cal/gram-atom K

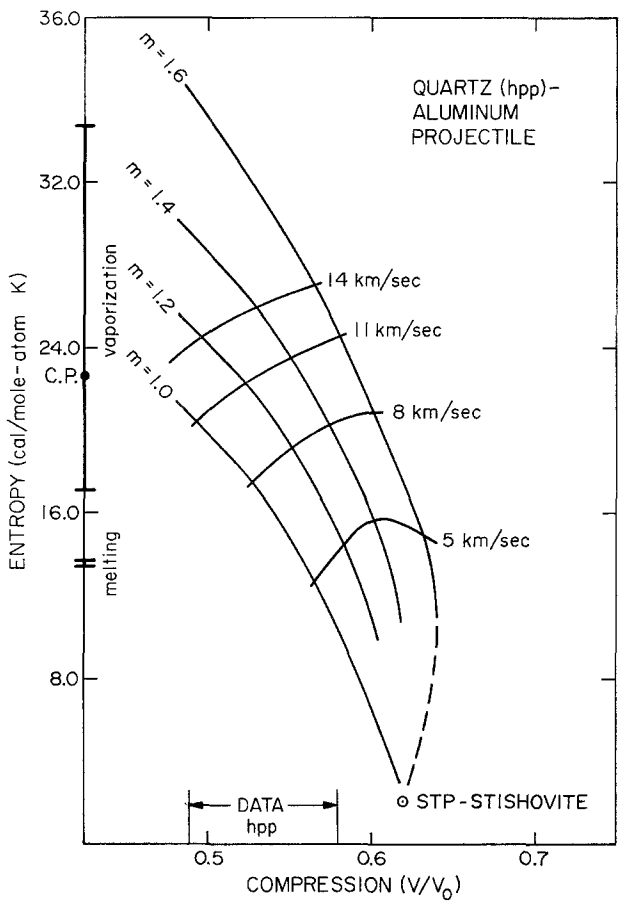

Fig. 8 a–b. Entropy versus compression for different distentions ($m = 1.0$ to 1.6) for SiO_2 (stishovite) for different projectile velocities; (a) aluminum projectiles, (b) iron projectiles. C. P. indicates vapor-liquid critical point entropy calculated from the theory of Young and Alder (1971). Range of Hugoniot data used is indicated by bracket in this and succeeding figures.

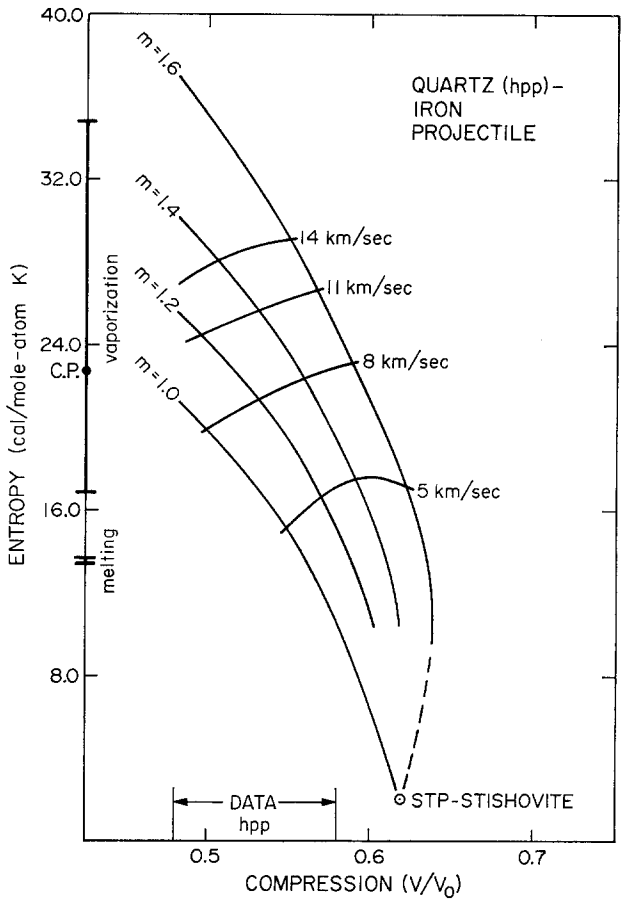

Fig. 8b.

The vaporization reaction for SiO_2 (Table IV) indicates that one mole of liquid will produce $\frac{3}{2}$ moles of hard spheres. The energy of formation of the liquid from the gas is taken to be -192 kcal/mole (Robie and Waldbaum, 1966), or in terms of moles of hard spheres, -128 kcal/mole.

The resulting values for the critical constants and critical point entropy, and the parameters for the critical van der Waal's isotherm, are given in Table IV.

7. Impact Conditions for Melting or Vaporization

The mechanical properties of objects which have, and undoubtedly still, impact the lunar surface probably range from those corresponding to very distended, frothy, NH_3-CH_4-CO_2 ices to those of iron. In order to examine the effect of the shock impedance of materials on the resulting shock state, we will consider the impact of lauminum and iron projectiles. Iron, of course, represents iron meteoroids, while

aluminum is grossly similar to silicates, or stony meteoroids, in both density, and shock properties.

Using the methods outlined in the previous section, the entropy (per mole of atoms) produced upon impact of aluminum and iron projectiles at speeds up to 9 km/s, and in several cases, 14 km/s, are shown relative to the compression of the lpp crystal volume in Figures 8–18 for a series of seven minerals and four rocks. The marked effect of varying the initial porosity, from zero to that corresponding to distentions of $m=2$ (bulk volume equals twice crystal volume) is demonstrated by the various curves. However, the condition of Equation (6), has in numerous cases, limited the range of distentions considered. From Table II it may be seen that the entropies required for melting, on a per mole of atoms basis, is roughly the same for all materials (12 to 17 cal/mole-atm K). Similarly, our calculations of the entropy change upon melting and vaporization, are in approximate agreement with empirical rules, generally

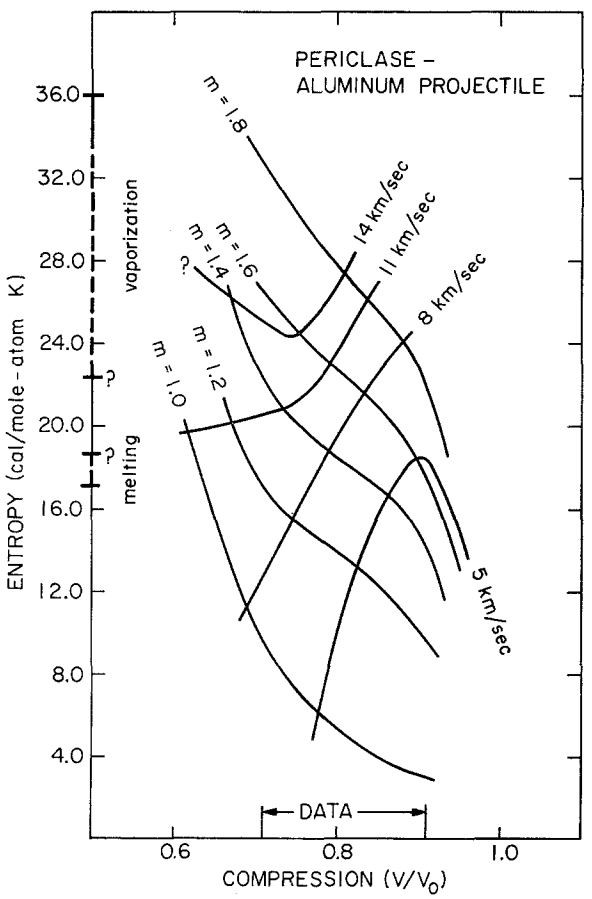

Fig. 9. Entropy versus compression for different distentions ($m=1.0$ to 1.8) for periclase (MgO) for different aluminum projectile velocities.

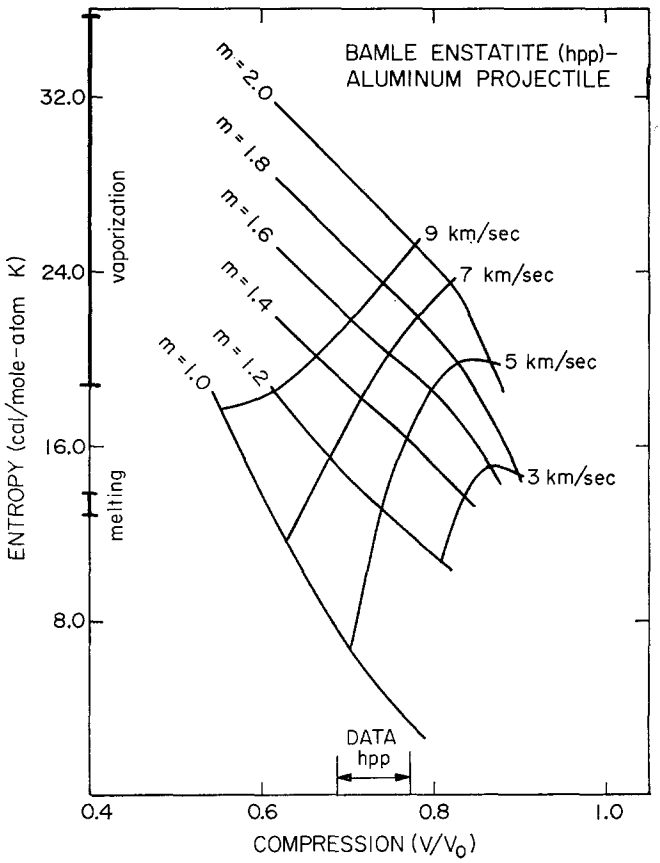

Fig. 10 a–b. Entropy versus compression for different distentions ($m = 1.0$ to 2.0) for Bamle enstatite (hpp) for different impact velocities, (a) aluminum projectile, (b) iron projectile.

applicable to elements and compounds, of Richardson and Trouton (Swalin, 1962) which predict values of 2 and 21 (cal/mole-atom K) for these, respectively.

Although the Hugoniot experiments on silicates and silicate-bearing rocks virtually all demonstrate the occurrence of phase changes, samples recovered from shock pressures as high as 1 mb, uniformly show that these changes are rapidly reversible and the recovered products are largely either amorphous (but perhaps unmelted), melted, or in the initial lpp. If we consider such amorphous phases as maskelynite, as being essentially a lpp, and we note the hpp such as coesite, stishovite, majorite and ringwoodite, make up less than, or most a few per cent, of the shocked material, the use of the thermal data for the lpp is justified. The behavior of some 11 different media for which calculations were carried out are described below.

8. Quartz

The hpp for which the calculations of Figure 8 are based, is stishovite, which starts to

form for shock states above ~140 kb. Recovery experiments verify this and also, because of the high temperature instability of stishovite, these provide implicit bounds on the maximum temperatures achieved (DeCarli and Milton, 1965). Complete transformation to stishovite is thought to occur above ~300 kb (McQueen *et al.*, 1963; Ahrens *et al.*, 1969a). Impact velocities of ~4 and ~6 km/s are needed to produce shock melting for iron and aluminum projectiles, while speeds of ~7 and ~8 km/s are required for vaporization of the single crystal ($m=1.0$) material. Of considerable interest is the maximum in the 5 km/s curves, from which it follows that impact into, α-SiO_2 with distentions of $m=1.4$ will produce more entropy, and hence more heating (at the projectile-target interface), than impact into either less, or more, distended material. This effect, although not occurring at easily attainable states in all materials, is apparently a general property of materials that can be described in terms of the Mie-Gruneisen equation of state (Equation (1)) (Ahrens, 1972). The observation that this optimum velocity occurs at slightly less compression that that corresponding to

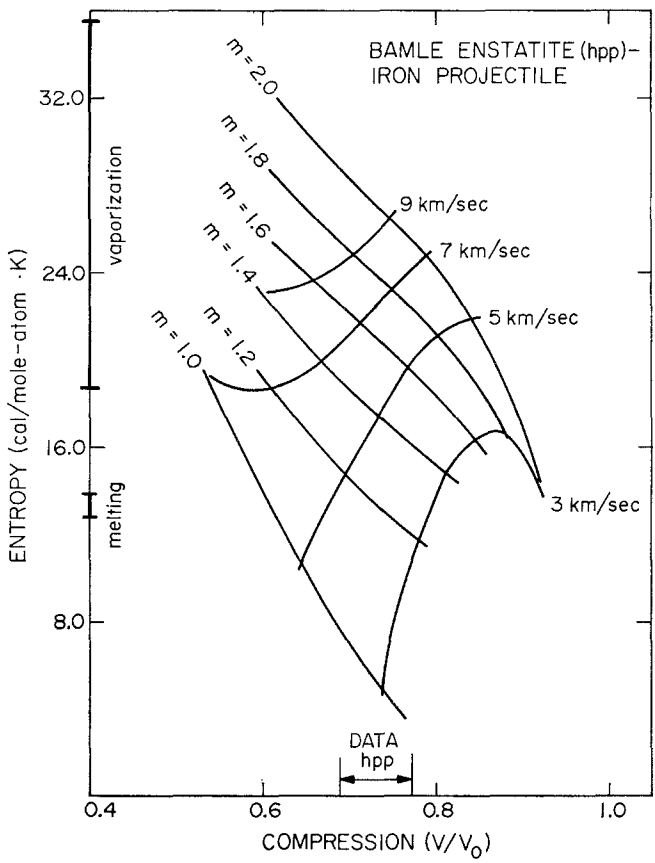

Fig. 10b.

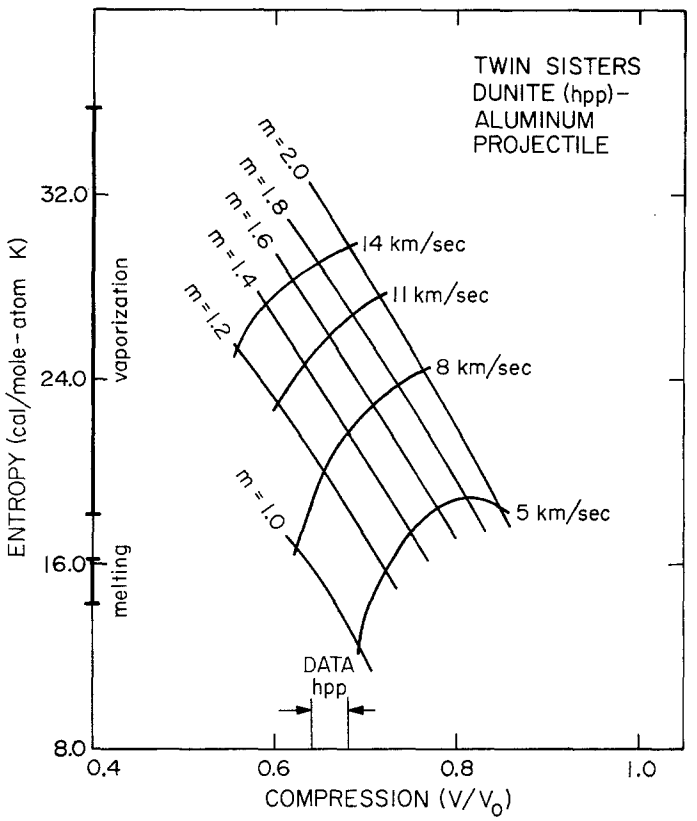

Fig. 11 a–b. Entropy versus compression for different distentions ($m = 1.0$ to 2.0) for Twin Sisters dunite (hpp), for different impact velocities, (a) aluminum projectile, (b) iron projectile.

complete transformation to the hpp is discussed with regard to the results for Bamle enstatite discussed below.

9. Periclase

This is the most refractory of the materials studied, and as shown in Figure 7, requires impact velocities of ~ 10 and ~ 12 km/s of an aluminum projectile to produce melting or vaporization respectively (of the single crystal). The optimum distention effect is quite marked. For a distension of $m \simeq 1.6$, approximately the same entropy is produced by a 5 km/s impact, as for a 10 km/s impact in the single crystal. The 11 and 14 km/s curves are known only very approximately because of our uncertainty to the value of the Gruneisen parameter at the high accompanying temperatures.

10. Bamle Enstatite

This material has a composition corresponding to $(Mg_{0.86}, Fe_{0.14})\,SiO_3$ which is

somewhat more Mg^{++} rich than most lunar pyroxenes. The Hugoniot data (Ahrens and Gaffney, 1971) demonstrate that this material undergoes a shock-induced phase change above $\sim$135 kb, possibly to a garnet-like structure. However, this transition must be readily reversible, as samples recovered from shock pressures as high as 250 kb indicate no significant disordering of this Fe^{++} distribution between M_1 and M_2 sites (Dundon and Hafner, 1971).

The calculated maximum in the entropy-compression curve, shown for 3 km/s projectiles for $m=1.6$, and for 5 km/s projectiles for $m=1.8$, should be interpreted with some caution as these maxima occur at compressions below the range of the hpp data for $m=1.0$. However, it may be that the mixed phase regime may be considerably narrower, in pressure and compression, in the case of the porous Hugoniot, as is reported in the case of the shock compression of porous quartz (Ahrens and Gregson, 1964). This is possibly the result of reaction rates becoming significantly greater at the higher shock temperatures of the porous material. Impact velocities of $\sim$6 and $\sim$8 km/s are required to induce melting in this mineral for iron and aluminum projectiles, respectively. Vaporization requires $\sim$7 and $\sim$10 km/s for aluminum and iron projectile velocities, respectively.

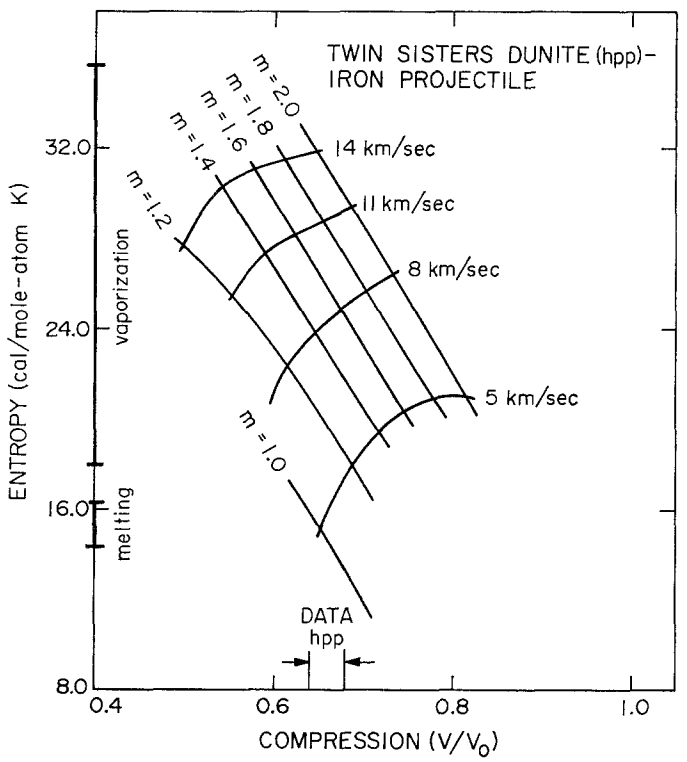

Fig. 11b.

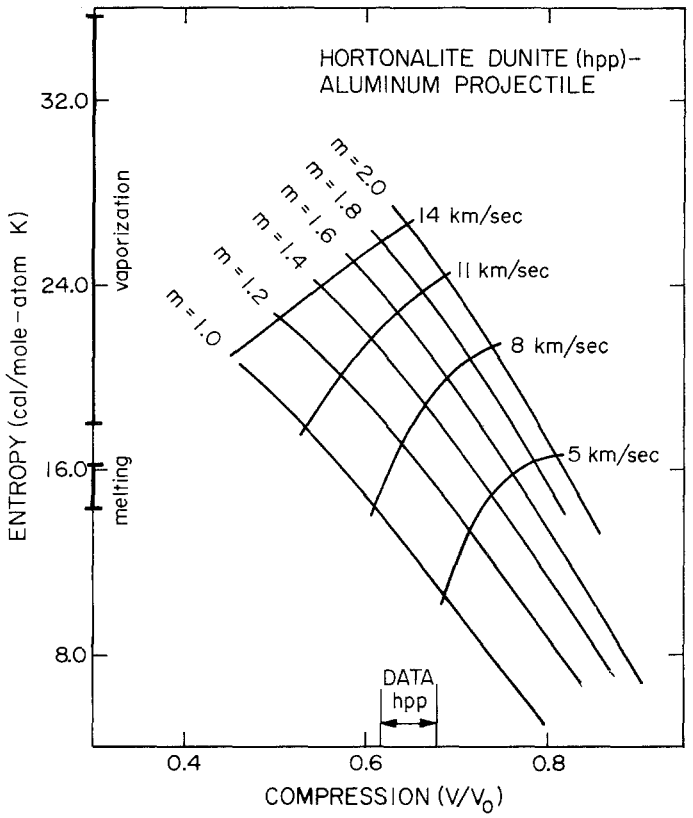

Fig. 12 a–b. Entropy versus compression for different distentions ($m = 1.0$ to 2.0) for Hortonolite dunite (hpp) for different impact velocities, (a) aluminum projectile, (b) iron projectile.

11. Twin Sisters and Hortonolite Dunite

The Hugoniots of these rocks were measured by McQueen *et al.* (1967). Both contain predominantly olivine, and have fayalite mole fractions of 0.12 and 0.53 for Twin Sisters and the Hortonolite material, respectively. The crystallographic nature of the shock-induced phases are not known with any certainty but it is likely that these have zero-pressure densities close to those of the mixed oxides (MgO, FeO and SiO_2 (stishovite). The hpp has been interpreted as probably forming in the Sr_2PbO_4 structure (Ahrens *et al.*, 1969a; Davies and Anderson, 1970). Shock melting requires impact speeds of ~ 7 and ~ 9 km/s and ~ 5 and ~ 8 km/s for the two dunites (Figures 11 and 12) in nonporous form. These indicated variations in the different composition dunites are probably artifacts of the calculations as they arise from the differing values of the Gruneisen parameter (Table I) used in the calculations and are probably less than those which can be attributed to the uncertainties in our knowledge of γ of the hpp(s). The impact velocities required for melting, which are really not well

determined, are very roughly consistent with the results of Vedder (1971), who experimentally studied the characteristics of laboratory-produced micro-impact craters in an olivine similar to that in the Twin Sisters dunite. For aluminum projectiles impacting at 5.8 km/s, his photographs show a ragged crater with little evidence of fluidity (i.e. melting), while a crater formed from a 13.1 km/s aluminum projectile

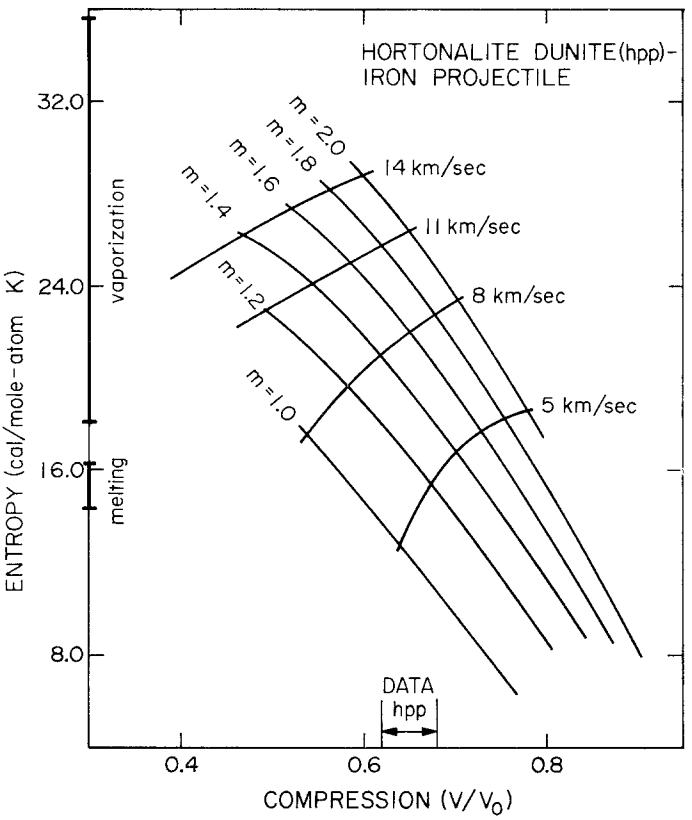

Fig. 12b.

shows considerable flow around the crater rim, presumably as a result of shock induced melting.

12. Oligoclase and Anorthosite

The exact nature of the hpp(s) of these minerals, although not explicitly known have been discussed in terms of transformation to the hollandite structure or disproportionation to jadeite, kyanite, grossalaite, and stishovite (Figure 3), (Ahrens *et al.*, 1969a,b). In any case, for the nonporous minerals, the present calculations specify shock-induced melting for aluminum and iron impacts at 6 km/s and 4 km/s, respec-

tively. Corresponding values for anorthosite are ~9 and ~8 km/s. The crater photographs of Vedder (1971) for oligoclase impacted at 6.9 km/s by aluminum suggest little, if any, melting while at 13.6 km/s obvious melting is shown. Similarly the results of Figure 4, using the energy method suggest a similar result, although the experimental uncertainties are large. On the other hand, ignoring the compositional

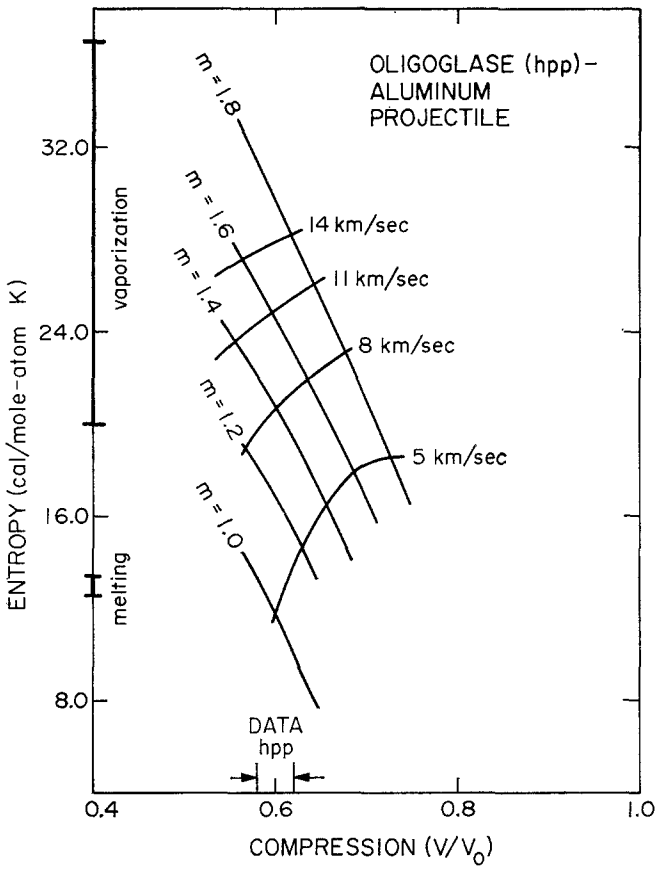

Fig. 13 a–b. Entropy versus compression for different distentions ($m = 1.0$ to 1.9) for Muskwa Lake oligoclase (hpp) for different impact velocities, (a) aluminum projectile, (b) iron projectile.

difference between anorthosite and oligoclase, the shock induced entropy production calculation, and the onset of shock-melting for anorthosite (Figure 14), agrees more closely with Vedder's result.

13. Centerville and Frederick Diabase and Vacaville Basalt

These rocks containing predominantly pyroxene and plagioclase are good analogies to several of the igneous rocks collected from the Moon. In the present calculations,

it is implicitly assumed that upon being engulfed by the shock, each of the minerals present, achieve the same entropy density. Observation of shocked rocks containing coexisting plagioclase and pyroxene (Chao, 1967) suggest that shock-induced melting occurs at considerably lower whole-rock pressures in plagioclase than in pyroxene. Since the present calculations indicate that for the nonporous materials, melting

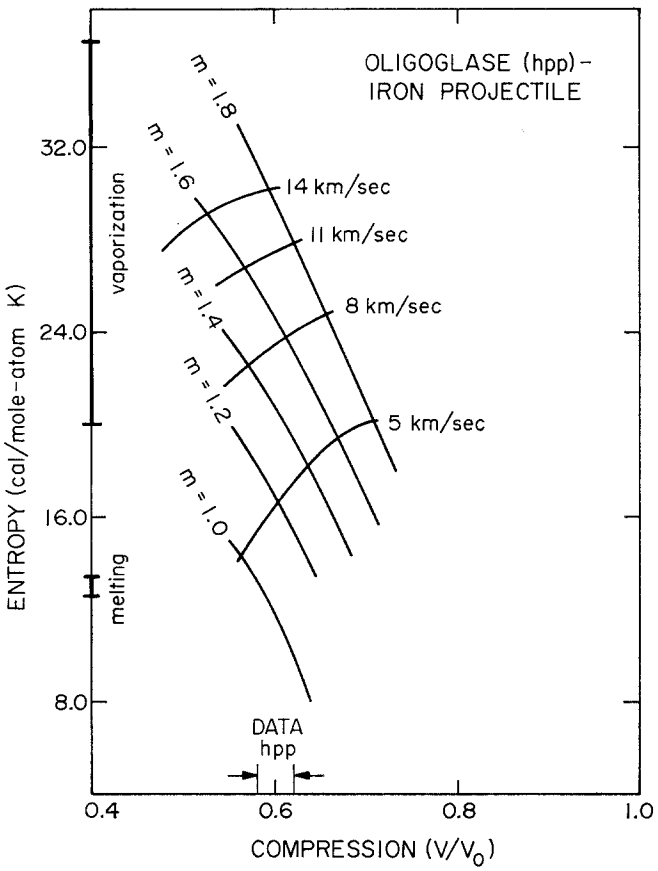

Fig. 13b.

occurs within both pyroxene and plagioclase at approximately the compression (V/V_0) of 0.55, the present results cannot take into account the differences in compressibility of pyroxene and plagioclase. Contrary to what is indicated in Figures 15–17, plagioclase being more compressible, should melt or become amorphous at lower impact velocities. The overall effect of increasing the porosity to values of distension, corresponding to the range observed in the lunar (soil), $m=1.4$ to 2.3, can be seen to drastically reduce the impact velocities which will produce melting. For iron and

aluminum projectiles, impact velocities in the range of 3 to 4 km/s will induce melting in a diabase-like rock at distentions corresponding to the lunar soil.

The Vacaville basalt, Figure 17, is also similar in composition to some lunar basalts, being somewhat more Na-rich. This rock contains 53% andesine, 31% augite, and 9% ilmenite-magnetite (plus 7% groundmass). Its somewhat lower zero-pressure density

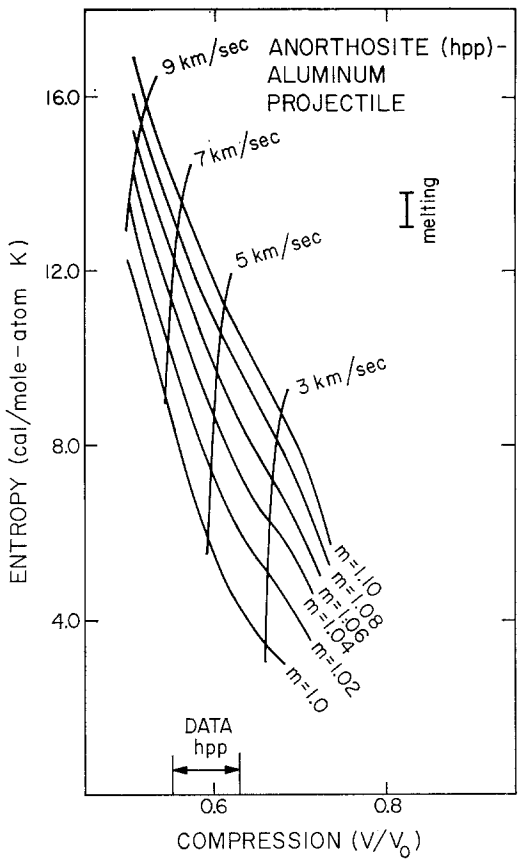

Fig. 14 a–b. Entropy versus compression for different distentions ($m = 1.0$ to 1.1) for anorthosite (hpp) for different impact velocities, (a) aluminum projectile, (b) iron projectile.

(2.82 g/cm^3) and a higher assumed value for the Gruneisen parameter, 1.39, gives rise to a somewhat higher entropy density than for the diabases, at a given impact velocity.

14. Granite

The impact conditions required for shock-induced melting of granitic rocks may be related to the formation of tektites. The velocities of iron and aluminum projectiles

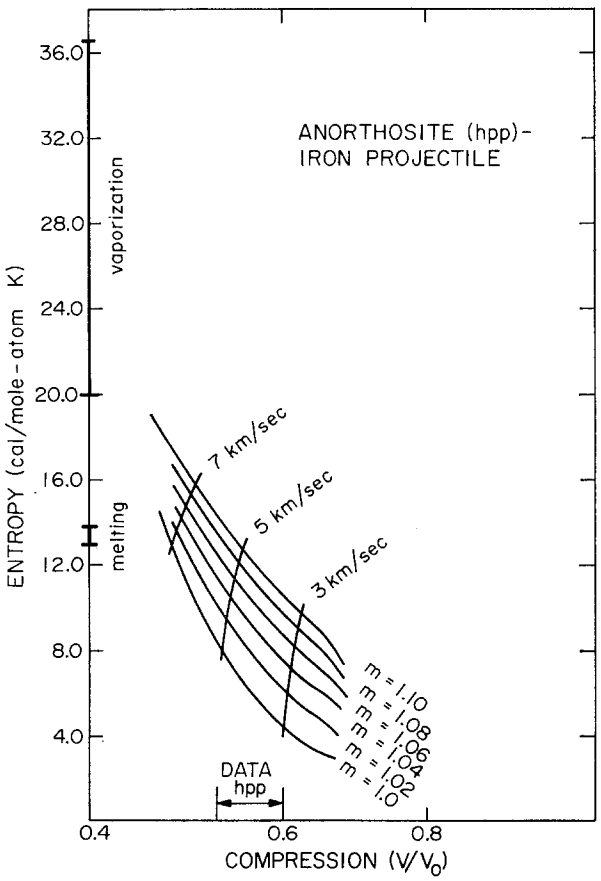

Fig. 14b.

required to induce melting are approximately 7 and 9 km/s for the solid material. As can be seen in Figure 10, our calculation suggest that, if entropy generation is uniform between the feldspar and quartz in a granite (which is likely since the compressibilities are similar) the potassium feldspar should melt at a slightly lower impact velocity than the quartz. The marked differences in the vaporization interval shown in Figure 18 are not known to be significant.

15. Summary

The thermodynamic state corresponding to the maximum shock pressure produced upon hypervelocity impact of a meteoroid with a planetary surface can be obtained by utilizing the appropriate Hugoniot curves of the impacting bodies in an impedance match solution (Rice *et al.*, 1958). Geometrical considerations may be used to demonstrate that the rock mass within the planetary surface exposed to this maximum

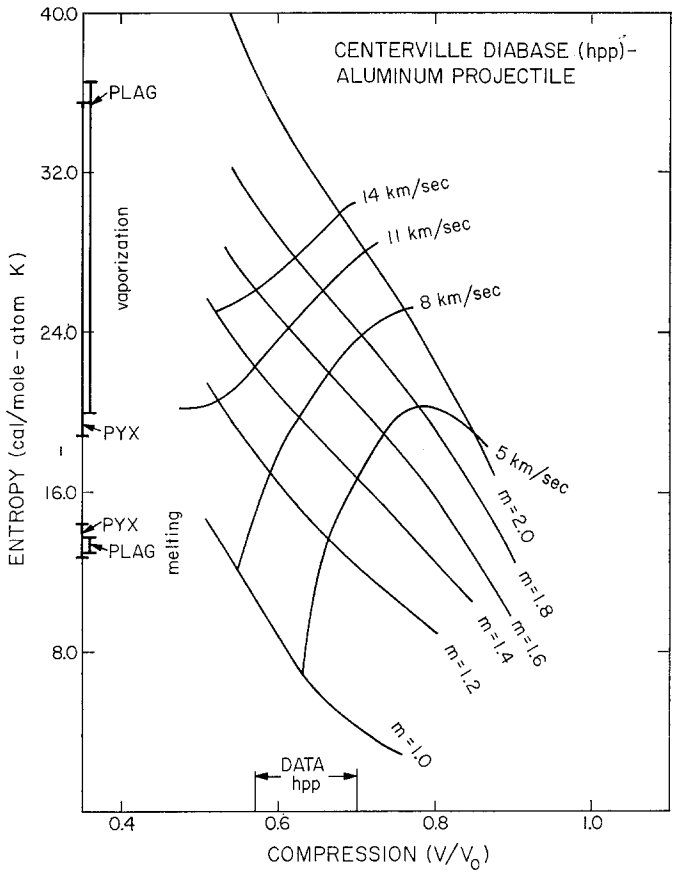

Fig. 15 a–b. Entropy versus compression for different distentions ($m = 1.0$ to 2.0) for Centerville diabase (hpp) for different impact velocities, (a) aluminum projectile, (b) iron projectile.

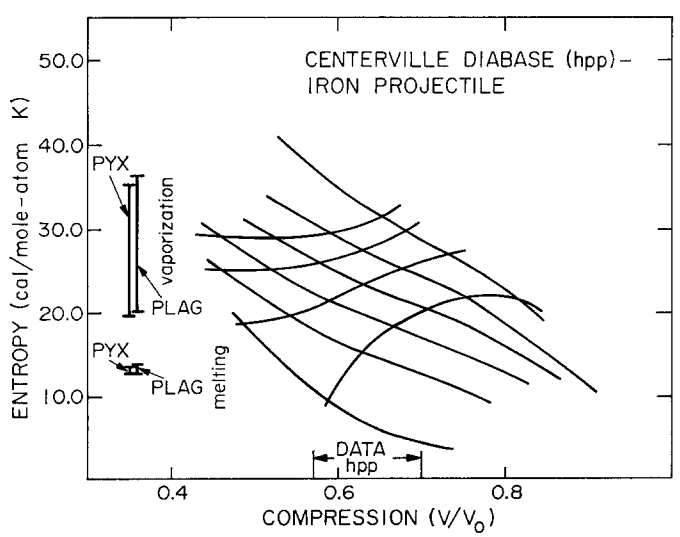

Fig. 15b.

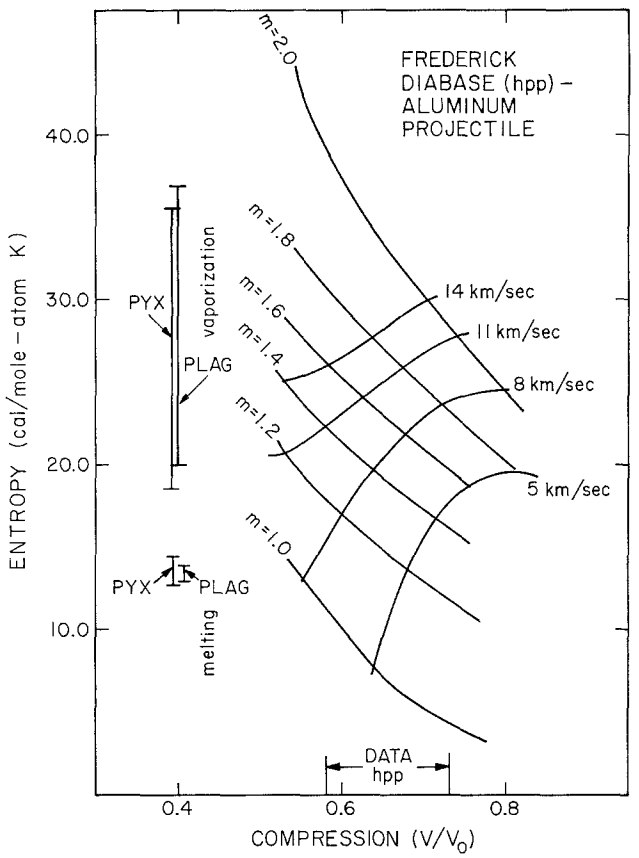

Fig. 16 a–b. Entropy versus compression for different distentions ($m = 1.0$ to 2.0) for Frederick diabase (hpp) for different impact velocities, (a) aluminum projectile, (b) iron projectile.

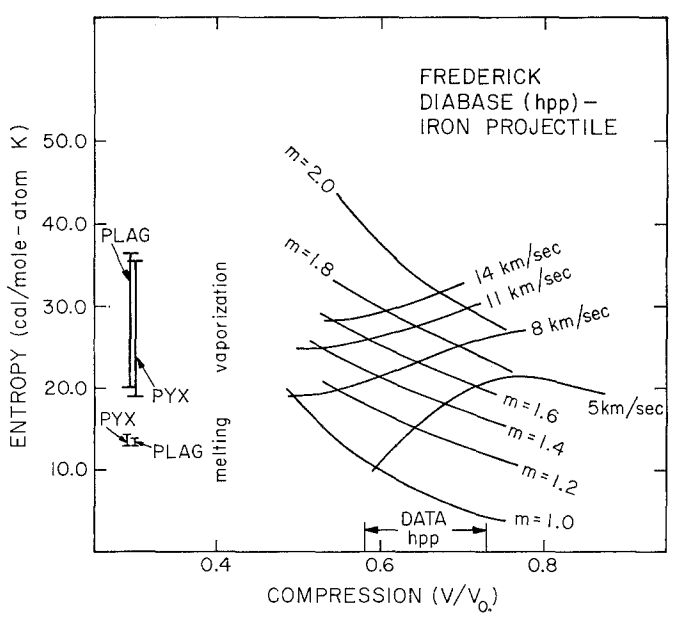

Fig. 16b.

shock pressure, is on the order of the mass of the impacting meteoroid. A large fraction of this intensely shocked material is known to be ejected as spray in the later stages of the impact process. It is likely that much of the glassy material, found in the lunar fines, comprising 10 to 60% of the grains, have such an impact origin. The description of the shock pressure, volume, energy and temperature state is relatively simply carried out by applying the Rankine-Hugoniot equations, and the Mie-Gruneisen equation of state. However, because of the phase transitions which take place in all of the silicates under shock compression, the calculation of the post shock state is less straightforward. In particular, the question of how fast an iron or stoney meteorite has to impact various minerals and rock-types in order to produce melting and vaporization can be attacked by either calculating the post shock energy (or enthalpy), or the post shock entropy gain, and then comparing the obtained values with high temperature thermodynamic and phase diagram data. Previous calculational efforts along these lines have largely concentrated on calculating the post energy using

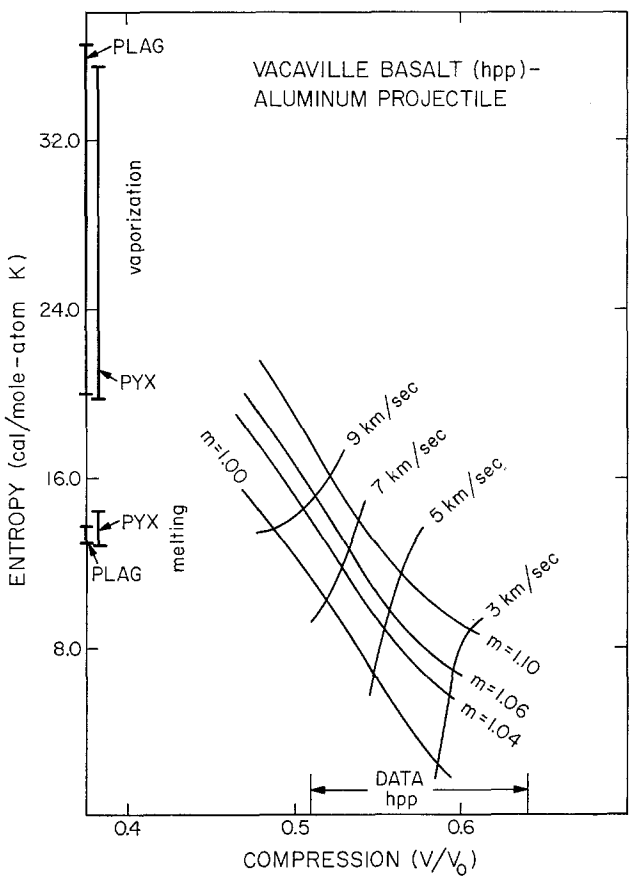

Fig. 17 a–b. Entropy versus compression for different distentions ($m = 1.0$ to 1.1) for Vacaville basalt (hpp) for different impact velocities, (a) aluminum projectile, (b) iron projectile.

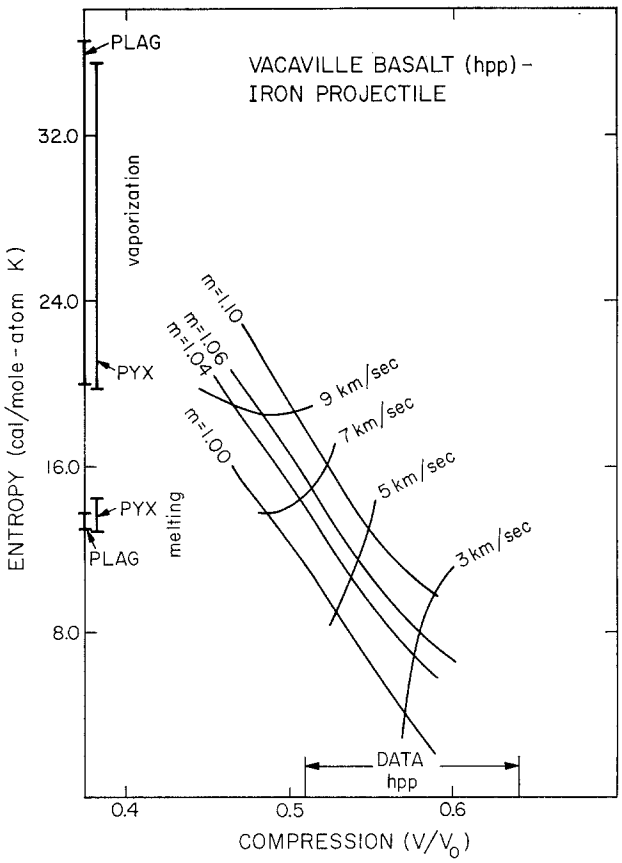

Fig. 17b.

theoretically constructing, or approximately deriving, release adiabats (the thermodynamic paths followed by the shocked material as its pressure is reduced to zero during the post-shock rarefaction). A limited number of measurements of release adiabat curves for silicates have demonstrated that, as a result of the phase changes in the silicates, the early theoretical estimates of the release adiabats (which often were closely approximated by the Hugoniot curve) will lead to serious underestimates of the irreversible work imparted to the mineral by the impact process. Using experimental release adiabat data for the Muskawa Lake plagioclase (ab, 0.75; an, 0.19; or, 0.06), post-shock energies and temperatures are calculated using energy cycles for adiabats centered at shock pressures up to 416 kb. Within the experimental uncertainties post shock temperatures as high as $\sim 1600\,^{\circ}C$ which are sufficient to melt this material, cannot be ruled out for single shocks in the range 250–300 kb. Although this is the range in which Milton and DeCarli (1963) observed maskelynite formation, their multiple shock experiments generated less entropy, and hence the present results are *not* necessarily inconsistent with the earlier suggestions that maskelynite (amor-

phous form of plagioclase) is a phase produced by solid-solid transformation. It also could be that maskelynite is merely a denser glass produced as a result of shock-induced melting at elevated pressures of the high pressure phase, although the lack of flow structure speaks against this hypothesis.

It is usually assumed that all the entropy production upon hypervelocity impact takes place, during the initial compression, and that upon subsequent rarefaction the specific entropy remains constant. Our tactic has been to calculate the entropy production during shocking, for a series of nonporous and porous rocks and minerals which occur on the Moon. We then compare these values with the magnitude of the entropy required for melting and vaporization at one atmosphere pressure. This method then requires only calculated shock temperatures and the one-atmosphere-pressure entropy values and, not, specific knowledge of the release adiabats. In the case of melting, entropy versus temperature data have been either measured or can

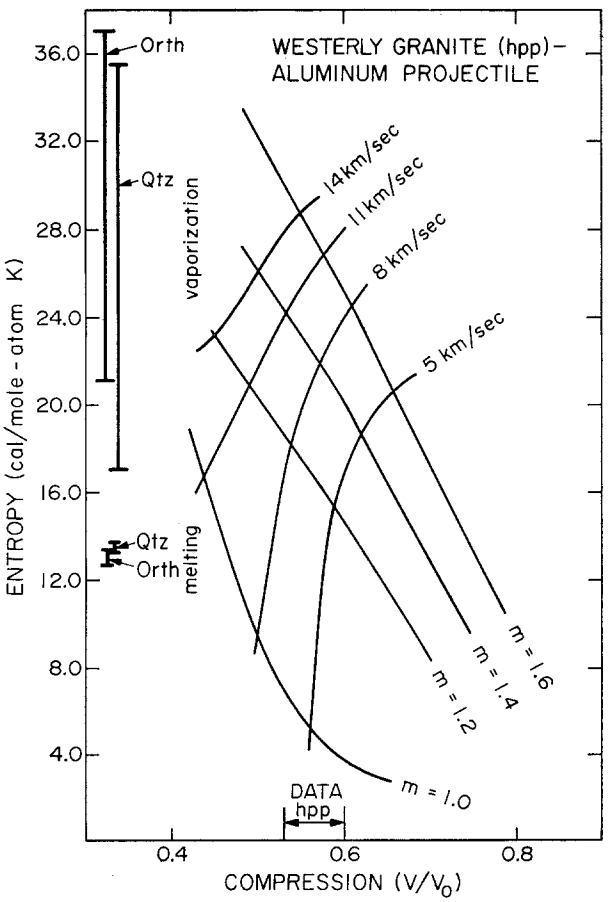

Fig. 18 a–b. Entropy versus compression for different distentions ($m = 1.0$ to 1.6) for Westerly granite (hpp) for different impact velocities, (a) aluminum projectile, (b) iron projectile.

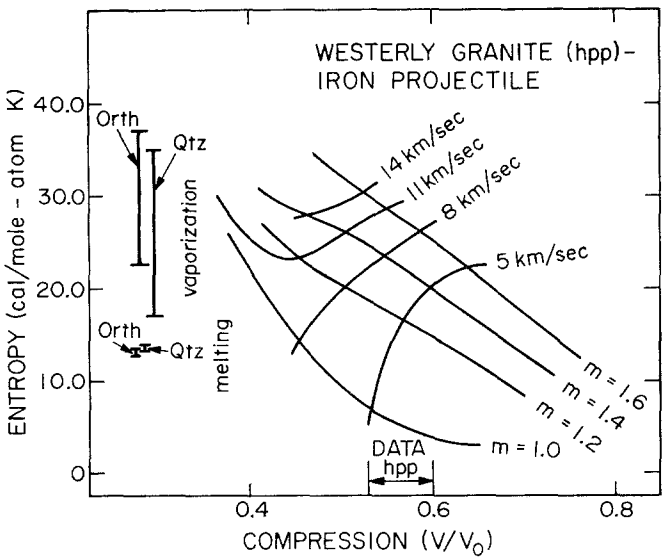

Fig. 18b.

be in a straightforward manner inferred. The entropy of incipient vaporization and the entropy of the completely vaporized species can be calculated from the data specifying the enthalpies of formation of the various oxides and application of statistical mechanical formulae. The entropy required to achieve melting on a mole of atoms basis, for all the silicates varies from $\sim$13 to $\sim$17 cal/mole K. The entropies of melting are generally less than 2 cal/mole K, while the entropies required for incipient vaporization and complete vaporization vary from 16 to 22 cal/mole K, and from 35 to 37 cal/mole K respectively. These latter values are relatively insensitive to the assumptions made concerning the oxide species in equilibrium with the liquid during the vaporization process.

In order to examine the effect of shock impedance on shock melting and vaporization, the specific entropies produced upon one-dimensional impact of aluminum and iron projectiles (representing silicate and iron meteoroids) with a series of target, silicates and rocks, were calculated. These results are sensitive to the values of the Gruneisen parameter one uses for the high pressure phases to calculate shock temperatures. Iron projectiles traveling at velocities of 4, 5 to 6, and 6 km/s will produce shock melting in quartz, plagioclase, olivine, and pyroxene (bronzite), in nonporous form, respectively. In the case of aluminum projectiles, speeds of approximately 6, 5 to 8, 8, and 10 km/s will result in melting in quartz and plagioclase, olivines, pyroxene (bronzite) and periclase. In the case of olivine and plagioclase these values are in good accord with the inferences which can be drawn from the limited photographic data on hypervelocity impact micro-craters recently reported by Vedder (1971). The impact speeds required for incipient vaporization are difficult to establish firmly because of the lack of data for the very high temperature, high pressure Gruneisen parameter and

the low pressure vapor equation of state. Calculated impact velocities for aluminum projectiles values vary from 7 to 8 km/s for quartz to 10 to 12 km/s for periclase to vaporize these minerals. The impact velocity required to melt and vaporize is shown to be drastically reduced by introducing porosity (to decrease the initial density) if local thermal equilibrium can be achieved. For example, iron and aluminum projectiles impacting a soil of diabasic or basaltic composition, having an initial bulk density in the range of 1.3 to 2.3 g/cm^3 (such as is observed on the surface of the moon), should induce complete melting at speeds as low as 3 and 4 km/s.

Acknowledgements

This research was supported by NASA grants NGL-05-005-105 and NGL-05-007-002 at the California Institute of Technology and University of California, respectively. We have profited from discussions with R. Taylor and T. Butkovich of the Lawrence Livermore Laboratory. We thank F. J. Kreiger of R. D. Associates for allowing us to use Figure 5 and P. S. DeCarli, R. G. Gibbons and E. C. T. Chao for helpful comments on this manuscript.

References

Ahrens, T. J.: 1972, *J. Appl. Phys.*, in press.
Ahrens, T. J. and Gaffney, E. S.: 1971, *J. Geophys. Res.* **76**, 5489–5498.
Ahrens, T. J. and Graham, E. K.: 1972, *Earth Planetary Sci. Letters*, in press.
Ahrens, T. J., Anderson, D. L. and Ringwood, A. E.: 1969a, *Rev. Geophys.* **7** 667–707.
Ahrens, T. J., Petersen, C. F. and Rosenberg, J. T.: 1969b, *J. Geophys. Res.* **74**, 2727–2746.
Ahrens, T. J. and Rosenberg, J. T.: 1968, in French, B. M. and N. M. Short, (eds.), *Shock Metamorphism of Natural Materials*, Mono Book Corp., Baltimore, pp. 59–81.
Brewer, L.: 1953, *Chem. Rev.* **52**, 1–75.
Butkovich, T. R.: 1967, 'The Gas Equation of State for Natural Materials', Lawrence Livermore Report, UCRL-14729.
Carter, J. L. and MacGregor, I. D.: 1970, *Science* **167**, 661–663.
Carter, W. J., Marsh, S. P., Fritz, J. N., and McQueen, R. G.: 1971, in *Accurate Characterization of the High Pressure Environment*, (ed. by E. C. Lloyd), NBS Spec. Publ. 326, pp. 147–158.
Chao, E. C. T.: 1967, *Science* **156**, 192–202.
Davies, G. F. and Anderson, D. L.: 1971, *J. Geophys. Res.* **76**, 2617–2627.
De Carli, P. S. and Jamieson, J. C.: 1959, *J. Chem. Phys.* **31**, 1675–1676.
De Carli, P. S. and Milton, D. J.: 1965, *Science* **147**, 144–145.
Dieke, G. H.: 1963, in *American Inst. of Phys. Handbook*, 2nd. Ed., Sect. 7.
Dundon, R. W. and Hafner, S. S.: 1971, *Science* **174**, 581–583.
Furakawa, G. T. and Douglas, T. B.: 1963, in *American Inst. of Phys. Handbook*, 2nd Ed., Sect. 4e.
Gibbons, R. V. and Ahrens, T. J.: 1971, *J. Geophys. Res.* **76**, 5489–5498.
Glass, B. P.: 1971, *J. Geophys. Res.* **76**, 5649-5657.
Horz, F., Hartung, J. B., and Gault, D. E.: 1971, *Earth Planetary Sci. Letters* **10**, 381–386.
Kieffer, S. W. and Kamb, B.: 1972, *Rev. Geophys.*, in press.
Kreiger, F. J.: 1967, 'The Thermodynamics of the Magnesium Silicate/Magnesium – Silicon Oxygen Vapor System', Rand Corp. Memorandum RM-5337-PR, April.
Lunar Sample Preliminary Examination Team: 1969, *Science* **165**, 1211–1227.
Lunar Sample Preliminary Examination Team: 1970, *Science* **167**, 1325–1339.
Lunar Sample Preliminary Examination Team: 1971, *Science* **173**, 681–694.
Lunar Sample Preliminary Examination Team: 1972, *Science*, in press.
Mayer, S. E. and Mayer, M. G.: 1940, *Statistical Mechanics*, John Wiley, New York.
McQueen, R. G., Marsh, S. P., and Fritz, J. N.: 1967, *J. Geophys. Res.* **72**, 4999–5036.

McQueen, R. G., Fritz, J. N., and Marsh, S. P.: 1963, *J. Geophys. Res.* **68**, 2319–2322.
Morgan, J. W., Laul, J. C., Ganapathy, R., and Anders, E.: 1971, *Science* **172**, 556–557.
Naumann, R. J.: 1971, *J. Appl. Phys.* **42**, 4945–4954.
Porter, R. F., Chupka, W. A., and Inghram, M. G.: 1955, *J. Chem. Phys.* **23**, 216–217.
Rice, M. H., McQueen, R. G., and Walsh, J. M.: 1958, in *Solid State Physics*, **6**, (ed. by F. Seitz and D. Turnbull), pp. 1-63, Academic Press, New York.
Robie, R. A. and Waldbaum, D. R.: 1968, *Geol. Survey Bull.* **1259**, 265 pp.
Shoemaker, E. M., Hait, M. H., Swann, G. A., Schleicher, D. L., Schaber, G. G., Sutton, R. L., and Dahlem, D. H.: 1970, *Geochim. Cosmochim. Acta Suppl. I, Proc. of the Apollo 11 Lunar Science Conf.*, **3**, pp. 2399–2412.
Shoemaker, E. M.: 1970, *Publ. Inst. Invest. Geol.* **24**, Universidad Barcelono, in press.
Swalin, R. A.: 1962, *Thermodynamics of Solids*, John Wiley, New York, 343 pp.
Trunin, R. F., Simakov, G. V., Podurets, M. A., Moiseyev, B. N., and Popov, L. V.: 1971a, *Izv. Earth Physics*, No. 1, pp. 13–20.
Trunin, R. F., Simakov, G. V., and Podurets, M. A.: 1971b, *Izv. Earth Physics*, No. 2, pp. 33–39.
Vedder, J. F.: 1971, *Earth Planetary Sci. Letters* **11**, 29–296.
Wackerle, J.: 1962, *J. Appl. Phys.* **33**, 922–937.
Walsh, J. M., Johnson, W. E., Dienes, J. K., Tillotson, J. H., and Yates, D. R.: 1964, 'Summary Report on the Theory of Hypervelocity Impact', General Atomic Report GA-5119, 66 pp.
Young, D. A. and Adler, B. J.: 1971, *Phys. Rev.* **3**, 364–669.
Zeldovich, Y. B. and Raizer, Y. P.: 1966, *Physics of Shock Waves and High Temperature Phenomena*, Academic Press, New York, Vol. II.